

¹ A Design for a Deep Underground Single-Phase
² Liquid Argon Time Projection Chamber for
³ Neutrino Physics and Astrophysics

⁴ March 31, 2015

Contents

2	1 Photon Detector	1
3	1.1 Introduction	1
4	1.2 Requirements and Goals	1
5	1.2.1 Beam-based physics	1
6	1.2.2 Proton Decay and Atmospheric Physics	2
7	1.2.3 Low-energy Physics	2
8	1.2.4 Required Performance	3
9	1.2.5 General Considerations	4
10	1.3 Photon Detector Prototype Designs	4
11	1.3.1 Cast or Bulk Doped Acrylic Bars	5
12	1.3.2 Fiber-embedded Bulk Acrylic Plate	7
13	1.3.3 LSU Photon detection panel production	7
14	1.3.4 Proof-of-Concept and Prototype Detector Results	9
15	1.3.5 R&D Work in Progress and Present Plans	11
16	1.3.6 Fiber Bundle with WS-coated Radiator	12
17	1.4 Silicon Photomultipliers	14
18	1.4.1 Requirements	17
19	1.4.2 Test Results	17
20	1.5 Mechanical Support	21
21	1.6 Photon System Readout Electronics	26
22	1.6.1 Reference Design	26
23	1.6.2 Alternatives	31
24	1.7 Photon Detector Calibration	33
25	1.8 Installation	38

¹ List of Figures

2	1.1	Probability of photon being detected in detectors when depositing energy	4
3	1.2	Schematic drawing of a light guide with its photosensors	5
4	1.3	LSU photon-detection panel	8
5	1.4	Light yield for the fiber LSU PD panels with alpha source in LAr	10
6	1.5	Summed charge plots of SiPMs in response to muon hodoscope trigger	11
7	1.6	Fiber-bundle PD prototype (early one-sided version)	13
8	1.7	SiPM signals as function of bias voltage in liquid nitrogen.	16
9	1.8	The diagram on the left shows the schematics of the PCB board, while the picture on the right shows the PCB as built. This PCB can accommodate three SiPMs for testing.	18
10	1.9	Picture on the left shows acrylic holder that secures SiPMs to the PCB while figure on the top right shows the entire assembly prior to lowering in the dewer. Orange cable delivers laser or LED light that shines on the SiPMs. Everything is secured to the wooden lid that closes the dewer.	19
11	1.10	SiPM SenSL C series gain tested in LN2 is shown on the right hand side. Excellent linearity over the entire overvoltage range observed. There is a significant change of gain with increasing bias voltage, effectively doubling between the minimum and maximum tested bias voltage. Clearly distinguished numbers of photoelectrons can be seen in the left hand figure.	19
12	1.11	SiPM SenSL C series dark rate with two different data runs in LN2. While dark rate increases for an order of magnitude, it is still less than 50 Hz even at the highest bias voltage setting.	20
13	1.12	SenSL C series SiPM afterpulsing fraction for 5 different SiPMs, with system being completely cooled down.	20
14	1.13	SenSL C series SiPM cross-talk measurement based on two separate runs in LN2. Cross-talk is a strong function of overvoltage and is very consistent between the runs.	21
15	1.14	Full APA frame with ten photon detectors mounted inside the frame	22

1	1.15 Photograph of 40 cm long bar-based prototype mounted in test frame	24
2	1.16 Mechanical assembly drawing of frame system	25
3	1.17 Blow up of APA fram showing PD insertion location	25
4	1.18 Slot and rail showing mounting location of photon detector	26
5	1.19 Block diagram of the photon detector signal processing system	27
6	1.20 Picture of the SSP module	29
7	1.21 Block diagram the SSP module	30
8	1.22 Concept of the UV-light calibration system	35
9	1.23 Diagrams of diffusers, their locations and UV light transport	35
10	1.24 Photon detector calibration module (PDCM) layout	36
11	1.25 Simulated light distributions of the 35-ton APA, two cases	37
12	1.26 Cable assembly for each photon detector readout channel.	39
13	1.27 Connection between the PD twisted pair cable and SiPM mounting board. .	40
14	1.28 Insertion of one PD paddle	40

List of Tables

2	1.1	Individual photon collection efficiencies	3
3	1.2	Light guide technologies	6
4	1.3	Physics requirements for the photon detector electronics	26

¹ Todo list

² In our 2012 CDR we started each chapter with: The scope of the (whichever)	
³ subsystem includes the design, procurement, fabrication, testing, delivery and	
⁴ installation of the mechanical and high voltage components of the (blah);	
⁵ followed by list of components – see the TPC chapter. At this late date, not	
⁶ sure it's worth it...	1
⁷ when?	2
⁸ clarify 'detector design can be found'	2
⁹	3
¹⁰ (need general TPC cell map with better description)	4
¹¹ Fuzzy at this size	5
¹² define 'baseline' here; do you mean 'reference design'?	7
¹³ reference?	7
¹⁴ indicate?	9
¹⁵ reference sec in r&d chap	11
¹⁶ ref?	12
¹⁷ make it longer?	12
¹⁸ opaque?	13
¹⁹ what? the fiber bundles?	13
²⁰ signals coming from wire wrapping? How about 'signals coming from wires on the	
²¹ APA frames'?	14
²² ref section	14
²³ check ref	23
²⁴ check ref	23
²⁵ No fig1 exists for: Block diagram of the photon detector signal processing system.	27
²⁶ fix	33

¹ Chapter 1

² Photon Detector

ch:photon

³ 1.1 Introduction

In our 2012 CDR we started each chapter with: The scope of the (whichever) subsystem includes the design, procurement, fabrication, testing, delivery and installation of the mechanical and high voltage components of the (blah); followed by list of components – see the TPC chapter. At this late date, not sure it's worth it...

⁴ Liquid argon is an excellent scintillating medium. With an average energy needed to produce a photon of 19.5 eV (at zero field) a typical particle depositing 1 MeV in liquid argon will generate 40,000 photons with wavelength of 128 nm. At higher fields this will be reduced but at 500 V/cm the yield is still about \sim 20,000 photons per MeV. Roughly 1/3 of the photons are promptly emitted after about 6 ns while the rest are emitted with a delay of 1100-1600 ns. LAr is highly transparent to the 128 VUV photons with a Rayleigh scattering length and absorption length of 95 cm and >200 cm respectively. The relatively large light yield makes the scintillation process an excellent candidate for determination of t_0 for non-beam related events. Detection of the scintillation light may also be helpful in background rejection.

¹⁵ 1.2 Requirements and Goals

¹⁶ 1.2.1 Beam-based physics

¹⁷ There are no requirements for the beam-based physics program, as the machine clock will provide a t_0 with roughly 10 μ s resolution. Given that the electron drift is 1.6

¹ mm/ μ s the uncertainty to the electron lifetime correction is small is
² when?

³ the beam timing is used. The photon system can be useful in determining the t_0
⁴ of cosmic ray events and events from radiological decays as well as giving a handle to
⁵ the location of beam events in the LAr volume with respect to fiducial boundaries.
⁶ The impact of the LAr scintillation light on the detector performance needs to be de-
⁷ termined, but it is not expected that the reduction in backgrounds for the oscillation
⁸ program will introduce additional requirements to the photon system design.

⁹ 1.2.2 Proton Decay and Atmospheric Physics

¹⁰ The photon detector system must provide the t_0 for non-beam related physics chan-
¹¹ nels if a correction for electron recombination during drift is to be applied. The
¹² requirements for electronics and hadronic energy resolution for the proton decay and
¹³ the atmospheric neutrino program are $1\%/\sqrt{E(\text{GeV})} \oplus 1\%$ and $30\%/\sqrt{E(\text{GeV})}$ re-
¹⁴ spectively. With these resolutions the collected charge must be accurately corrected
¹⁵ for recombination. Therefore the photon system must provide a t_0 for particles with
¹⁶ >100 MeV with $>95\%$ efficiency in the fiducial volume of the detector.

¹⁷ 1.2.3 Low-energy Physics

¹⁸ Supernova events will produce neutrinos down to about ~ 5 MeV. Studies have es-
¹⁹ timated the momentum resolution for 5 MeV electrons to be 20% using only TPC
²⁰ information and assuming a highly efficient trigger and an electron lifetime of 5 ms.
²¹ The impact of various detector resolutions on the physics potential of LBNE has not
²² been studied in detail. At present there is no strong requirement that the energy
²³ resolution be better than 20%, so no requirement on the photon system trigger effi-
²⁴ ciency is set at this time. However it is clear that if a detector design can be found,

²⁵ clarify ‘detector design can be found’
²⁶

²⁷ the energy resolution would greatly improve. A goal of the photon detection
²⁸ R&D is to develop a system with the lowest possible threshold for a reasonable cost.
²⁹ At the start of final design, a final decision as to the configuration will need to be
³⁰ made based on cost and added physics capability.

¹ 1.2.4 Required Performance

² To achieve the physics goals in the previous section the performance of the photon
³ detection system must be understood. The prototype readout electronics described
⁴ in Section 1.6 have been shown to detect the single photoelectron (p.e.) signals
⁵ associated with the late scintillation light but future versions may sacrifice this ability
⁶ to mitigate high channel costs. It is assumed that the physics goals of the photon
⁷ detection system will be met using the prompt scintillation light.

⁸ The performance, or overall photon collection efficiency, is given by the following,
⁹ where it is assumed only prompt light is collected:

$$\frac{N_{pe}}{MeV} = N_{128} \cdot \epsilon_{geom} \cdot \epsilon_E \cdot \epsilon_{mesh} \cdot \epsilon_{conv} \cdot \epsilon_{capt} \epsilon_{tran} \cdot \epsilon_{QE} \quad (1.1)$$

¹⁰ The efficiencies leading to the overall number of photo-electrons collected by the
¹¹ photon detection system, $\frac{N_{pe}}{MeV}$, are given in table ^{Table-Eff} ??.

Table 1.1: Individual photon collection efficiencies

Factor	Description	Value	Comments
ϵ_{geom}	geometric acceptance	0.0036	historical average
ϵ_E	field correction	0.6	500 V/cm
ϵ_{mesh}	TPC wire shadowing	.83 (30-150°)	^{HimmelMesh} falls off sharply [?]
ϵ_{conv}	TPB conversion	1	^{Bib:gehrman} see ref. [?]
ϵ_{capt}	waveguide incident	0.5	about half converted photons travel into waveguide
ϵ_{tran}	waveguide transmission	TBD	prototype dependent
ϵ_{QE}	SiPM QE	.31	SensL b-series

¹² Using Equation 1.1 it is seen that to detect a 2 p.e. signal, likely to be dis-
¹³ criminated from noise, the transport efficiency is 1.2%. Of course this value is very
¹⁴ position-dependent, as the geometric acceptance, wire shadowing and transport cor-
¹⁵ rections all depend on the location of the event. Figure ^{fig:photon map} 1.1 shows the probability of
¹⁶ (?)

¹⁷ MeV energy deposition being detected in the photon detectors.

¹⁸ The TPC wire mesh shadowing is also quite location-dependent as photon an-
¹⁹ gles, relative to the wire plane, lead to rapid loss in transmission below 30° and

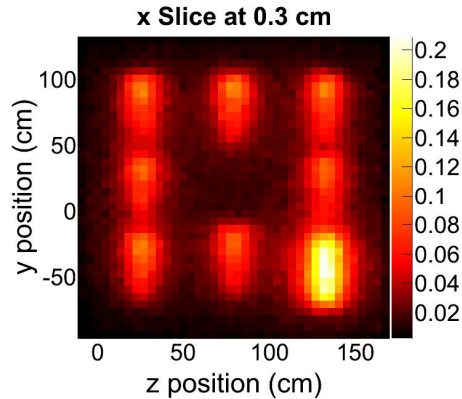


Figure 1.1: Photon map giving the probability of photon being detected in the photon detectors when depositing energy at map location.

(need general TPC cell map with better description)

`fig:photon_map`

1 greater than 150° . Lastly, the photon detector paddles themselves can have position-
 2 dependent response to incident photons due to the attenuation length of the wave-
 3 uide. The photon detector simulation, which is nearing stable operation, will be able
 4 to better estimate the efficiencies coming from geometric acceptance correction.

5 **1.2.5 General Considerations**

6 In the event that higher photon collection efficiencies can be achieved it should be
 7 possible to improve the energy resolution of the detector by adding the photon yield
 8 to the electron yield information. However this requires several orders of improve-
 9 ment in light collection efficiency, so it is beyond the scope of the present design.

10 **1.3 Photon Detector Prototype Designs**

11 All designs considered for the photon detector have been based on the use of wavelength-
 12 shifting coating, or bulk doping, of plastic materials coupled to silicon photomulti-
 13 pliers (SiPMs). The reference design, described in Section 1.3.1, utilizes a coated
 14 acrylic waveguide coupled to SiPMs. Alternate designs, described in the following
 15 sections, have been developed in an effort to optimize coverage, cost and attenuation
 16 length.

1.3.1 Cast or Bulk Doped Acrylic Bars

¹ sec_bars
² The reference design for the photon detection system is based on light guides that
³ are coated with wavelength shifter. The 128-nm scintillation photons from liquid
⁴ argon interact with the wavelength shifter on the light guide surface and 430-nm
⁵ light is re-emitted in the bar. The light guide channels the light to photodetectors
⁶ at its end.

⁷ A schematic drawing of a light guide with its photosensors is shown in Figure 1.2.
⁸ The prototype light guides are bars with a footprint 2.54 cm × 0.6 cm. The concept
⁹ is described in Ref. [?].

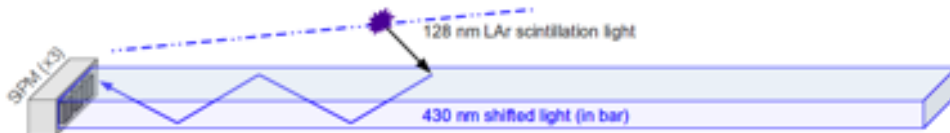


Figure 1.2: Schematic drawing of a light guide with its photosensors. The bars have embedded wavelength shifter (WLS), either TPB or bis-MSB. Three SiPMs collect the waveshifted photons that have been internally reflected to the bar's end.

Fuzzy at this size

¹⁰ The wavelength shifter converts incident VUV scintillation photons to 430 nm
¹¹ photons inside the bar, with an efficiency of $\sim 50\%$ for converting a VUV to an opti-
¹² cal photon [?]. A fraction of the waveshifted optical photons are internally reflected
¹³ to the bar's end where they are detected by SiPMs whose QE is well matched to
¹⁴ the 430-nm waveshifted photons. The light guides were made with one of two wave-
¹⁵ length shifters: the conventional TPB (1,1,4,4-tetraphenyl-1,3-butadiene) and the
¹⁶ less expensive alternative bis-MSB (1,4-bis-(o-methyl-styryl)-benzene). Preliminary
¹⁷ studies with a VUV monochromator show that the two wavelength shifters compare
¹⁸ favorably in their waveshifting efficiency [?]. A testing program is currently underway
¹⁹ to compare their relative performance in liquid argon.

²⁰ A team at Indiana University is studying prototype light guides made with three
²¹ different technologies. These technologies are listed in Table 1.2.

²² The clear acrylic bars (a) are made from blanks of commercially available Lucite-
²³ UTRAN cast UVT acrylic sheet that has been laser-cut and diamond-polished into
²⁴ bars of the proper size. Lucite-UTRAN has the longest attenuation length of the
²⁵ acrylics tested [?]. The Eljen¹ bars (b and c) are commercial light guides that
²⁶ are doped with J2 green fluor (equivalent to Y11). Two types of light guides were

¹<http://www.eljentechnology.com>

Table 1.2: Light guide technologies

Label	Light Guide Technologies
(a)	clear acrylic, dip-coated
(b)	doped Eljen PVT light guide, dip-coated
(c)	doped Eljen polystyrene light guide, dip-coated

ab:lightGuides

1 purchased from Eljen. The light guides (b) were fabricated from polyvinyl toluene
 2 (PVT); these are the standard Eljen product EJ-280. The quantum efficiency of
 3 the fluorescent dopant in EJ-280 is 0.86, so the second shift in wavelength does not
 4 markedly degrade the photon detector efficiency. The light guides (c) were fabricated
 5 from polystyrene; these light guides were ordered because PVT bars can craze if
 6 cooled too rapidly. Although the PVT light guides may be brighter, no instance of
 7 crazing has ever been observed in polystyrene light guides.

8 For the acrylic light guides, the WLS must be embedded in the plastic at the
 9 bar's surface so that 128-nm scintillation photons can generate optical 430-nm pho-
 10 tons within the volume of the plastic. Otherwise the VUV photons will not be
 11 trapped by the light guide. For the Eljen bars, the wavelength shifter can either be
 12 embedded in the plastic, as with the acrylic, or it can be deposited on a plate or
 13 film placed in proximity to the light guides. The J2 wavelength shifter then converts
 14 the resulting 430-nm photons inside the light guides where they are channeled to the
 15 photodetectors.

16 To embed the WLS at the surface of the light guides, a “dip-coating” process was
 17 developed at Indiana University. Before the WLS was applied to the acrylic bars,
 18 the bars were annealed at 80°C for one hour. (The Eljen bars were not annealed.)
 19 The WLS was dissolved in the organic solvent dichlormethane (CH_2Cl_2). For these
 20 waveguides 5 g of wavelength shifter was dissolved in 1,000 gm of DCM. A series of
 21 experiments showed that this concentration was optimum. A bar was first dipped
 22 into the WLS mixture for 15 seconds and then removed. It was then hung in the dark
 23 for at least two hours to dry. Once dry, the ends of the bars were flycut. Currently
 24 designs are being fabricated that put an acrylic plate painted with WLS or a thin
 25 film impregnated with WLS in front of the Eljen light guides.

26 In summer 2015 these designs will all be tested side-by-side at the TallBo dewar
 27 facility at Fermilab under uniform, low-contamination conditions. In addition to
 28 the designs described above, these tests will include photon detector designs from
 29 Colorado State University and Louisiana State University. This experiment will
 30 compare the relative performance and the absolute efficiency for all designs scaled

¹ to 1.5 m.

² 1.3.2 Fiber-embedded Bulk Acrylic Plate

³ The LSU team has developed a VUV photon detector design for a large LAr detector
⁴ that overcomes some of the shortcomings of the present LBNE baseline
⁵ define ‘baseline’ here; do you mean ‘reference design’?

⁶ photon detectors. The LSU photon detector design allows for coverage of a very
⁷ large area, thereby increasing the geometrical acceptance of the photon detectors.
⁸ The number of required SiPMs and readout channels per unit detector area covered
⁹ with photon detection panels has been significantly reduced to keep the overall cost
¹⁰ for the photon detection system at or below the present design while increasing the
¹¹ geometrical acceptance.

¹² The photon detection system consists of a TPB-coated acrylic panel with an
¹³ embedded S-shaped wavelength shifting (WLS) fiber. The fiber is read out by two
¹⁴ SiPMs, which are coupled to either end of the fiber, and serves to transport the
¹⁵ light over long distances with minimal attenuation. The double-ended fiber readout
¹⁶ has the added benefit of providing some position dependence to the light generation
¹⁷ along the panel by comparing relative signal sizes and arrival times in the two SiPMs.
¹⁸ Figure 1.3 shows a drawing of the layout and a photograph of a prototype photon
¹⁹ detection panel in the test stand at LSU. The incoming 128-nm VUV Ar scintillation
²⁰ light will be converted by the thin TPB layer on the acrylic panel and re-emitted
²¹ with wavelength peaking at 430 nm in an isotropic way. About 50% of the light is
²² emitted into the acrylic panel where some fraction will be absorbed by the WLS fiber
²³ and converted to light with a peak intensity of about 480 – 500 nm. The green light
²⁴ exiting the fiber is well matched to the peak photon detection efficiency of typical
²⁵ SiPMs.

²⁶ 1.3.3 LSU Photon detection panel production

²⁷ The photon detection panels are produced from 0.25-inch-thick sheet UVT acrylic
²⁸ and cut to size. For a first series of prototypes the acrylic panel dimensions were
²⁹ chosen to closely match the area of four bars of the LBNE baseline
³⁰ reference?

³¹ photon detection system. The groove is cut with a CNC mill in several passes to
³² achieve good groove surface quality, which is important for good light transmission
³³ from the bulk acrylic to the fiber. The panels are dip coated with TPB and left to dry

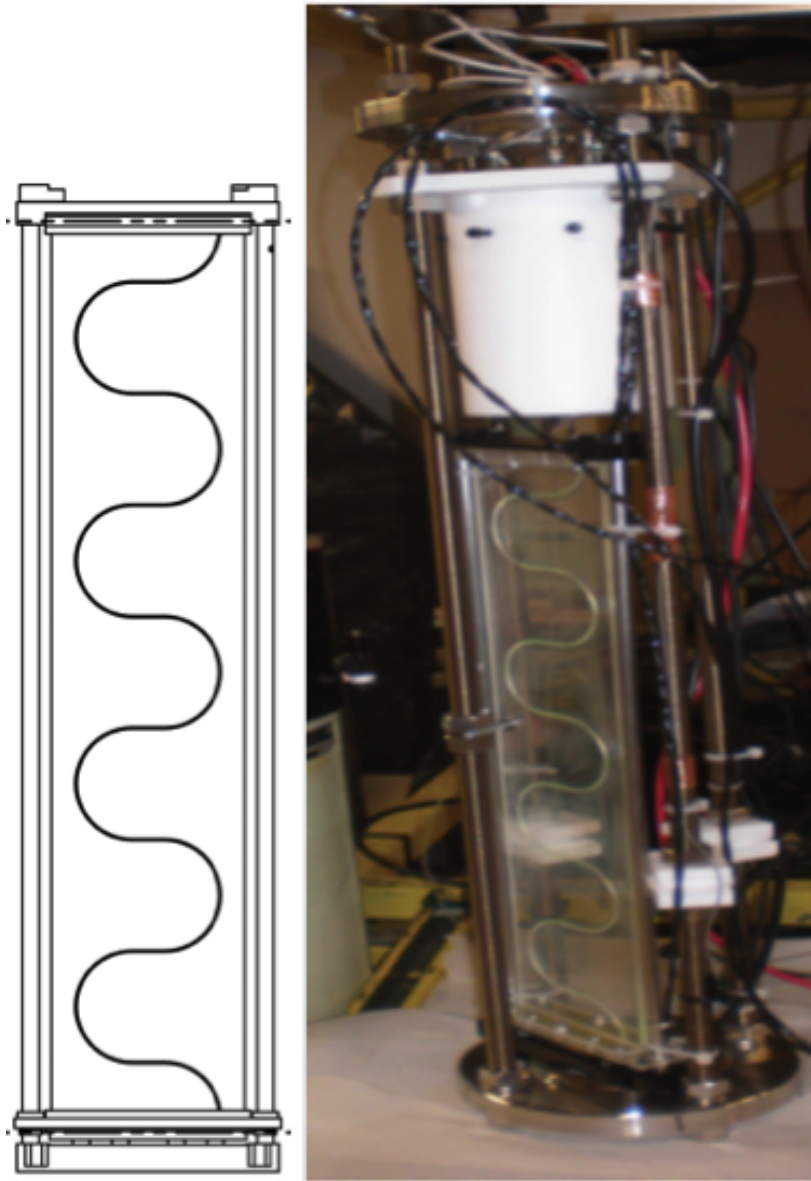


Figure 1.3: LSU photon-detection panel. Technical drawing of a $20'' \times 4.33''$ acrylic panel with embedded WLS fiber (left) and picture of a prototype in test set-up at LSU (right) with the same dimensions.

fig:1-LSU

1 prior to insertion of the WLS fiber. Panels with two and three layers of fibers inserted
2 and glued into the groove have been produced. Fiber ends are cut and polished. The
3 resulting acrylic panels are then inserted into a custom-made mechanical frame. The
4 end caps of the mechanical frame house one SiPM on either end. The presently used
5 $6 \times 6\text{mm}^2$ active-area SiPMs are spring-mounted to ensure good contact between the
6 active area and the fiber ends. The leads of the SiPMs are connected to a small PCB
7 onto which $\sim 2\text{-m-long}$ twisted-pair coax cables are soldered to supply the SiPM
8 with a bias voltage and to read out signals. The other cable ends are typically
9 connected to pre-amplifiers before leading to a DAQ system. Components for the
10 photon detection panels are inspected at all stages of the manufacturing process for
11 quality. Due to the small number of panels produced to date, no quantitative quality
12 control parameters have been defined yet. Proper connectivity of the fully assembled
13 units are tested in a setup at LSU using a LED flasher. If LED light signals are
14 seen, the panel is successively immersed in gaseous argon (GAr) along with an alpha
15 source. The observation of scintillation light originating from alpha particles and
16 cosmic rays penetrating the GAr volume allows for a relatively quick quality-control
17 check of a completed photon detector at room temperature.

18 **1.3.4 Proof-of-Concept and Prototype Detector Results**

19 Several photon detector panels of $20 \times 4.33\text{in}^2$ have been produced and two have
20 been tested in a LAr test stand at CSU. The detectors submitted to the cold test
21 have three and two embedded fibers, respectively, but are otherwise produced in the
22 same way. The data taken in LAr included self-triggered alpha source scans as well
23 as cosmic runs with a muon hodoscope providing a trigger for near-vertical muons
24 penetrating the LAr volume.

25 **Alpha source runs:** The alpha source was placed at a distance of about 1 inch
26 in front of the center line of the photon panel and moved to 20 different positions
27 spaced about 1 inch apart from neighboring positions. At each position 5000 signal
28 traces were recorded and measurements were repeated for three of the positions to
29 check the reproducibility of the measured light yield. Figure 1.4 shows results for
30 both successively measured panels. The red and blue dots show the mean light yield
31 values in units of p.e. (photo electron equivalents = no. of fired SiPM pixels) for the
32 SiPM on the top and bottom end of the panel as function of source position. Green
33 dots show the sum of both channels. The summed signals provide

34 indicate?

1 a very uniform detector response for the entire panel, independent of the alpha
 2 source position. The data also indicate good reproducibility for the doubly measured
 3 positions. The three-fiber panel shows about 50% more light when compared to
 4 the two-fiber panel, which is in good agreement with expectations. It needs to be
 5 pointed out that the LAr purity was not monitored and that measurements for the
 6 two panels were performed sequentially after refilling the dewar with LAr. However,
 7 the liquid argon for both measurements came from the same batch, which motivates
 8 the assumption that the purity for both measurements was very similar.

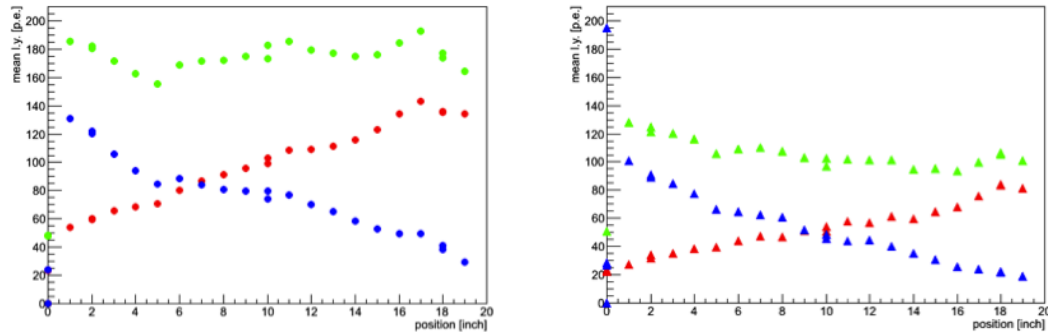


Figure 1.4: Light yield for the three (left) and two (right) fiber LSU photon detection panels in response to a 1-in distant alpha source in LAr. Red and blue symbols represent the mean light yield over 5000 trigger events from a single SiPM each and green points represent the summed signal from both SiPMs.

fig:2-LSU

9 **Cosmic trigger runs:** Two $1'' \times 10''$ wide scintillator counters were placed above
 10 and below the dewar to form a muon hodoscope and to select near-vertical muons
 11 traversing the LAr volume. The three-fiber LSU panel and one LBNL/Elgin Bis-
 12 MSB doped polystyrene bar of LBNE baseline dimensions and read out by three
 13 SiPMs were simultaneously inserted in the LAr. The setup allowed the study of
 14 the response of these photon detectors to scintillation light created by penetrating
 15 cosmic muons. A detailed quantitative comparison of the relative light yield was
 16 not possible with this setup due to large systematic uncertainties in the position
 17 dependence of the scintillation light generation by the triggering cosmic muons. A
 18 qualitative comparison of the detector responses, taken as the signal sum of three
 19 and two SiPMs for the Elgin bar and the LSU panel, respectively, shows comparable
 20 light yields as shown in Figure 1.5.

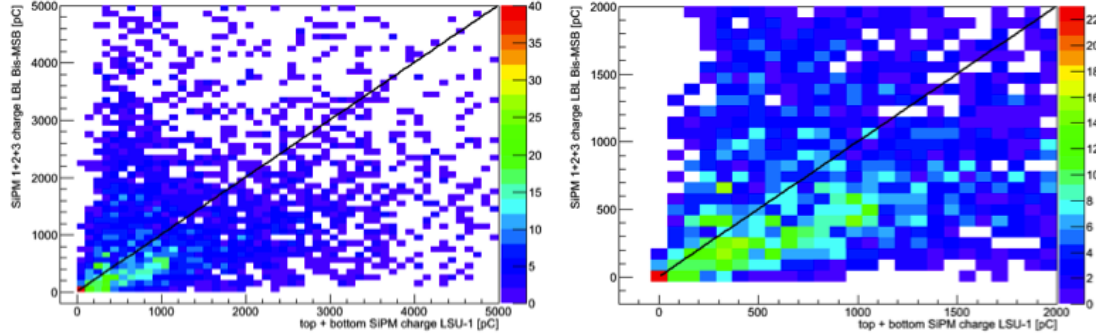


Figure 1.5: Scatter plot of the summed charge of three SiPMs coupled to the LBNL/Elgin Bis-MSB doped bar and the summed charge of two SiPMs for the three-fiber LSU panel in response to an external muon hodoscope trigger. The right plot shows a zoomed version of the left plot.

fig:3-LSU

1.3.5 R&D Work in Progress and Present Plans

After the construction and proof-of-principle test of the LSU-style photon detection panels several 2.17-m-long and 110-mm-wide (=4.33") panels were manufactured to demonstrate the scalability of the design. At the time of writing, tests in the large LAr dewar at CSU are in progress. The team is performing alpha source scans and cosmic muon runs. The alpha source scan runs are arranged such that the source illuminates two photon detectors at the same time. This setup facilitates quantitative and relative light yield comparison between different photon detector designs in the same LAr bath with a well-defined VUV light source.

Manufacturing and testing of wider panels is under consideration to maximize the photon detector panel area in the DUNE LAr far detector. The goal is to cover the entire anode plane assembly (APA) area with photon detectors embedded into the APA frame. Another important measurement goal is to establish the energy threshold of the photon detection panels. A study will be conducted for the photon detectors presently installed in the 35t detector

reference sec in r&d chap

using Michel electrons. The 35t detector contains one of the three-fiber LSU photon detection panels. In addition, performing alpha source runs in a well-controlled and monitored LAr setup may provide information on the particle energy threshold for observation of VUV scintillation light. The measurement of a photon detector panel's light yield as function of the source distance is another key measurement to

1 estimate the response and sensitivity of the full photon detection system in a LAr
2 detector. Results will be useful to validate MC simulations. We are exploring options
3 to perform these tests in the large dewar setup at CSU or alternatively in the TallBo
4 setup

5 ref?

6 at FNAL.

7 The TPB coating procedure of the acrylic panels has not yet been optimized and
8 improvements may be possible. A systematic study is foreseen to identify parameters
9 in the TPB dip and in the evaporation coating procedure to maximize the light yield
10 of resulting samples. These tests will be performed on small $10 \times 10 \text{ cm}^2$ acrylic
11 panels with a U-shaped embedded WLS fiber. On the software and analysis side,
12 tools are being improved to study position dependence for alpha-source run data
13 using relative signal timing and size. Furthermore, it is planned to continue work on
14 analysis algorithms to identify the late light component from argon scintillation.

15 Finally, early exploratory work on wallpapering the TPC cathode planes with
16 TPB coated Tetratex foils and observing the shifted light with suitably installed
17 photon sensors in combination with light collector cones will be pursued and explored
18 more rigorously to provide timely results.

19 **1.3.6 Fiber Bundle with WS-coated Radiator**

20 A reduction in attenuation length has been observed in acrylic waveguides that have
21 been doped with TPB. One possible way to address this reduction would be to
22 populate the PD system with half-length paddles. However, this would lead to an
23 increase in the number of readout channels, and readout electronics is the driving
24 cost of the photon detector system. While it may be possible to combine readout
25 channels to mitigate the increase in overall number, a more desirable solution would
26 be to address the attenuation length issue.

27 by ‘address’ do you mean make it longer?

28 To mitigate the reduced attenuation length in TPB-doped or -coated acrylic and
29 polystyrene, the CSU group has been developing an alternative design based on UV-
30 to-blue wavelength shifting fiber (Y11) that has not been treated with TPB. A thin
31 ^{fig:fiber bundle}TPB-coated acrylic radiator located in front of a close-packed array of WLS fibers.
32 Figure 1.6 shows a photograph of the fiber-bundle prototype.

33 The VUV photons are incident on the TPB-coated plastic radiator and roughly
34 half of the photons converted in the radiator are incident on the fiber bundle. These
35 photons are then directed onto SiPMs at one end. The Y11 fiber (from Kuraray



Figure 1.6: Photograph of fiber-bundle PD prototype (early one-sided version). The thin TPB-coated radiator is mounted on top of the prototype in the image.

fig:fiber_bund

1) have mean absorption and emission wavelengths of about 440 nm and 480 nm
2 respectively. The attenuation length of the Y11 fibers is given to be greater than
3 3.5 m at the mean emission wavelength, which allows production of full-scale (2.2-m
4 length) photon detector paddles.

5 First prototypes of this design utilized two rows of fibers with a reflector behind
6 the double row used to redirect the unabsorbed \sim 400 nm photons back through the
7 two rows. Data taken at the CSU Cryogenic Detector Development Facility (CDDF)
8 and the Fall 2014 FNAL Tallbo test showed that the front row of fibers collected
9 twice as much light as the back row, thus only a single row design can be considered
10 — this is currently under development. The current design utilizes two single rows
11 of fibers back-to-back with layers of

12 opaque?

13 Tyvek diffuse reflector between them.

14 In this design

15 what? the fiber bundles?

16 would face into different TPC cells, allowing additional information to be used
17 in the disambiguation of the TPC signals coming from wire wrapping on the APA

¹ frames.

² signals coming from wire wrapping? How about ‘signals coming from wires on
the APA frames’?

³ If the walls of the detector were to be covered with TPB-coated material shifting
⁴ the VUV photon to blue, the WS-fiber in this design could capture the emitted
⁵ light, offering a further benefit. Further study is required to determine the effect
⁶ these enhancements would have on the physics reach of the detector.

⁷ To fully exploit this approach several design optimizations need to be examined,
⁸ including the following:

- ⁹ • TPB coating thickness on thin radiator
- ¹⁰ • Double-ended readout; if the fibers are read out from both ends and the corresponding channels are ganged onto one readout channel, an increase in channel output can be obtained without significant cost
- ¹¹ • Use of custom-doped fibers to best match the QE response of the SiPMs and the emission spectrum of the TPB
- ¹² • Removal of the radiator and coating the TPB directly onto the outer fiber-cladding of the Y11 fibers. Since the fibers are double-clad it may be the case that the attenuation length of the fibers is not altered by the TPB application. The geometry of the close-packed fiber row may lead to increased photon (400 nm) collection

²⁰ The cost of this design is comparable to that of the bar-based design but is slightly
²¹ more complex to fabricate — although the Y11 fibers are commercially available,
²² which is an attractive feature. The engineering aspects of the design will be discussed
²³ in the appropriate section of this chapter.

²⁴ ref section

²⁵ 1.4 Silicon Photomultipliers

²⁶ Silicon Photomultipliers (SiPMs) have been selected as photon detectors for the far
²⁷ detector LArTPC photon detection system. SiPM is a photo detection device sensitive
²⁸ to single photons with excellent linearity range in collecting multiple photons.
²⁹ SiPM consists of a large avalanche photodiode (APD) array built on a common silicon
³⁰ substrate. APDs operate in Geiger mode.

1 SiPMs have been developing at a very fast pace in recent years, in response to
2 the needs of medical industry. As a result, the price of SiPMs has gone down, while
3 their performance has greatly improved. There are a number of characteristics that
4 make SiPMs an attractive choice as photo-detectors for the PD system.

- 5 • High photon-detection efficiency (PDE) up to 40-50% at the peak detection
6 wavelength.
- 7 • High intrinsic gain at ranging from 105 to 107 depending on the overvoltage.
- 8 • Low dark rate at cryogenic temperatures - less than 50 Hz even at the maximum
9 overvoltage.
- 10 • Insensitive to external magnetic field.
- 11 • Gain vs. overvoltage is extremely linear.
- 12 • Low cost per sensitive area compared to small cryogenic photomultiplier tubes
13 (PMTs).
- 14 • Small dimensions allow simple, compact and robust design.
- 15 • No need for high voltage (HV) power.
- 16 • Bias voltage required is typically less than 100 V, and even less than 30 V in
17 some cases, resulting in low peripheral costs.
- 18 • Gain and PDE remain high at cryogenic temperatures.

19 In short, SiPMs demonstrated performance that is comparable to traditional
20 PMTs, but at a significantly reduced cost. As a result, they have become a photon-
21 detector of choice for PD system of the far LArTPC detector.

22 The main risk associated with using SiPMs is that generally they have not been
23 designed for operation at LAr temperature. None of the SiPM data sheets show nor
24 guarantee their performance at cryogenic temperatures. This was the main motive
25 for testing SiPMs at LAr temperatures. Tests performed in the last two years have
26 mostly been done using LN2 as it has similar temperature (10 K below LAr), but it
27 costs much less.

28 There is a number of SiPM manufacturers on the market such as SenSL, Hamamatsu,
29 KETEK, AdvanSiD, CPTA (Photonique), Philipis, Novel Device Laboratory
30 (NDL), Zecotek, Voxtel, Amlification Technologies, Excelites, etc, but only a fraction

of them offer SiPMs that are suitable for PD system- large area ($6 \times 6 \text{ mm}^2$ or $3 \times 3 \text{ mm}^2$), large fill factor, pin or surface mount and no housing. We have conducted an exhaustive search in 2012 of suitable SiPMs, although one should keep in mind, that in this rapidly developing field, manufacturers come up with new, improved models every year in most cases. As result of 2012 search, sample SiPMs were obtained from SenSL, Hamamatsu, CPTA and AdvanSID. Samples

There are many SiPM suppliers on the market. In the initial round of tests, we tested models from SenSL (MicroSM-600-35-X13), Hamamatsu(MPPC S10985-100C), CPTA (SSPM-0710G9MM) and AdvanSID (ASD-SiPM3S-P), as we had success in obtaining suitable models from these four companies. In this test, SiPMs were cooled in liquid nitrogen and signal output as a function of overvoltage was recorded. Laser light pulse at 400 nm wavelength was used a light source. Results can be seen in Fig. ??.

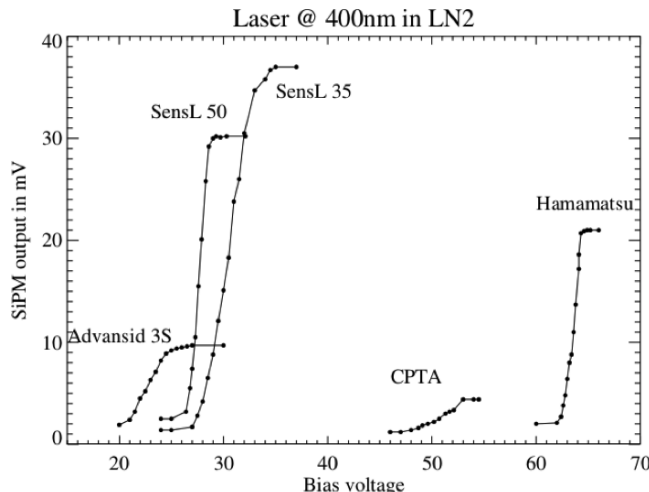


Figure 1.7: SiPM signals as function of bias voltage in liquid nitrogen. Liquid nitrogen has 10 K lower temperature than liquid argon, making the measurement applicable. In all cases there is a significant increase in gain with increasing bias voltage, but difference in gain among different samples is clearly visible.

fig:laser400

Based on these initial tests, the follow up tests focused on SenSL and Hamamatsu models. This decision was partially driven by the high price quotes received at the time from AdvanSiD and CPTA.

Shortly after initial tests, SenSL came up with a new model (MicroFB-600-35-SMT followed by improved MicroFC-600-35-SMT) and most of the tests have been done on the SenSL models. Hamamatsu's MPPC S12895- 0404-PB50 has been

1 on the market for a long time and Indiana group measured very high cross-talk and
2 afterpulsing rates. Hamamatsu came up with a new, improved model in 2015, S13360,
3 that will be tested in 2015 and compared with SenSL models.

4 **1.4.1 Requirements**

5 PD system requires high sensitivity photo-detectors to detect argon scintillation light,
6 despite its excellent scintillation yield due to a very small surface area of the PDs.
7 The late scintillation light in argon represents 2/3 of the total scintillation light, but
8 it is spread over 1100 - 1600 ns, making the individual late light signals very small
9 in average.

10 SiPM characteristics from the data sheets satisfy these requirements in general.
11 Thus, it is important to verify that similar performance is observed at LAr tempera-
12 tures in terms of high gain, sensitivity to single photoelectrons, high PDE, linearity
13 of the response, stability of breakdown voltage, long-term stability, low afterpulsing
14 and low cross-talk. In addition, SiPMs must have low dark rate and mechanical
15 robustness as they undergo cryogenic cooling and cycling. Finally devices must have
16 low cost and we need to identify at least two suitable choices to avoid sole source
17 issues.

18 Institutions designing different PD prototypes (Indiana University, Colorado State
19 University and Louisiana State University) have conducted a number of tests of PDs
20 with SiPMs. Additional, specifically targeted tests have been conducted at Louisiana
21 State University (LSU) and University of Hawaii (UH) in recent months. Importance
22 of selecting the best photo-sensors for the PD motivates the need for parallel tests
23 conducted at both LSU and UH. Such approach will ensure important cross-checks
24 and reduce possible testing biases.

25 **1.4.2 Test Results**

26 In the last 18 months, we have built a test setup for SiPM evaluation, that includes
27 Belle experiment electronics to power and record signals from SiPMs. More recently,
28 we have designed a new board similar to SenSL testing board (to address noise
29 problems and low amplification of the Belle board critical at low light levels) that
30 is currently being used to conduct dark rate and single photoelectron study. Fig ??
31 shows the layout of the new testing board and picture of the actual circuit as built.

32 As previously mentioned, tests focused on Hamamatsu and SenSL produced 8
33 SiPMs. However, Indiana University group found out that Hamamatsu SiPMs are
34 placed in a dewar inside a copper plated dark box and cooled with LN2. SiPMs are

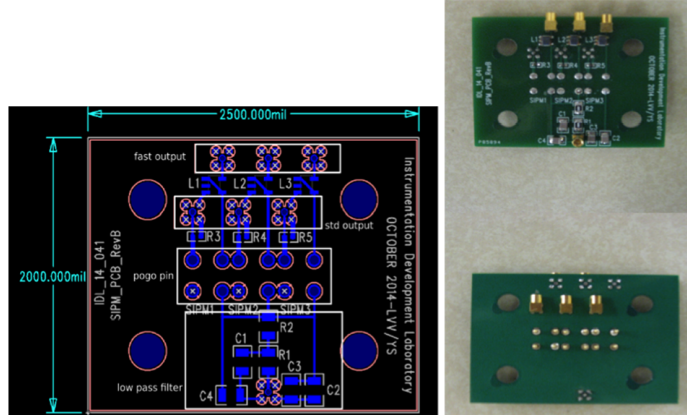


Figure 1.8: The diagram on the left shows the schematics of the PCB board, while the picture on the right shows the PCB as built. This PCB can accommodate three SiPMs for testing.

`fig:sipm_schem`

1 held in place on the PCB with acrylic holder as shown in the Fig ??.

2 To address the issue of different contraction rates of materials in LN₂ that pro-
3 duced mechanical damage to some of the SiPMs, a PCB board with spring loaded
4 POGO pins is used (based on the previous design by the Colorado State University
5 group) to provide contact to SiPMs and hold SiPMs in place with acrylic housing
6 rather than solder joints. We have also acquired special cryo rated, compact MMCX
7 connectors, as the solder joints of the signal and power wires have been breaking
8 from repeated usage.

9 The SiPM bias voltage is delivered via POGO pins and SiPM signal is sent via
10 POGO pins to the DAQ. The signal is amplified via two inline low noise amplifiers
11 and read out by oscilloscope. SiPMs are illuminated by a 1 ns long laser pulses from
12 the tunable wavelength laser system. Laser light intensity is regulated with a Fine
13 Laser Intensity Controller (FLIC), a computer controlled system allowing us to tune
14 laser intensity through several orders of magnitude with various stages, important
15 for linearity measurements. Signal waveforms from Waverunner LeCroy oscilloscope
16 are recorded and analyzed afterwards.

17 We have also noted that the SiPMs require lower bias voltage when cooled in LN₂,
18 which requires determination of the optimal operating voltage at LAr temperature
19 as dark rates also increase with bias voltage. Additional tests showed excellent gain
20 at cryogenic temperatures as can be seen from the tests conducted on the SenSL C
21 series SiPM MicroFC-600-35-SMT (previous M and B series also tested) shown in
22 Fig ?? along with clearly distinguished pulses for 1, 2, 3 and 4 photoelectron pulses.

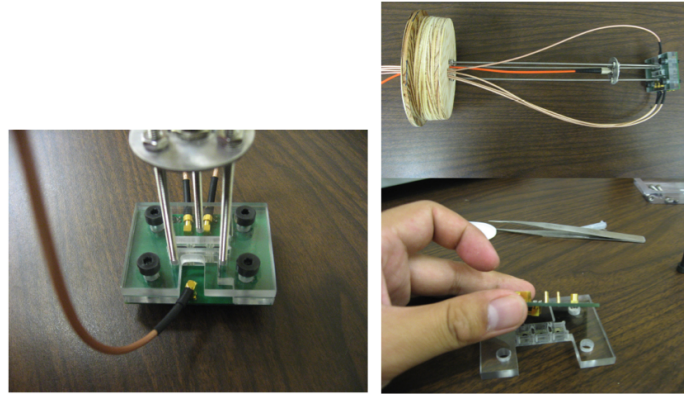


Figure 1.9: Picture on the left shows acrylic holder that secures SiPMs to the PCB while figure on the top right shows the entire assembly prior to lowering in the dewer. Orange cable delivers laser or LED light that shines on the SiPMs. Everything is secured to the wooden lid that closes the dewer.

fig:sipm_mount

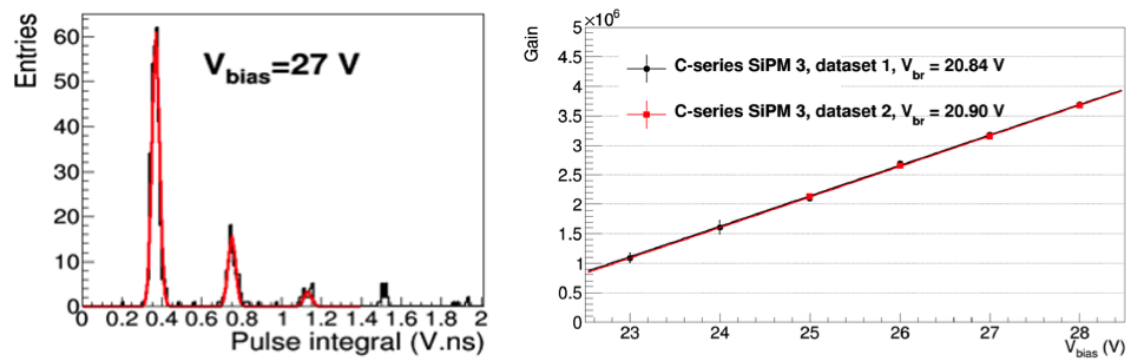


Figure 1.10: SiPM SenSL C series gain tested in LN₂ is shown on the right hand side. Excellent linearity over the entire overvoltage range observed. There is a significant change of gain with increasing bias voltage, effectively doubling between the minimum and maximum tested bias voltage. Clearly distinguished numbers of photoelectrons can be seen in the left hand figure.

fig:sipm_gain

1 The dark rate increases significantly with bias voltage, but the overall rate is very
 2 small when SiPMs are cooled down to 80 K as can be seen in Fig. ??.



Figure 1.11: SiPM SenSL C series dark rate with two different data runs in LN2. While dark rate increases for an order of magnitude, it is still less than 50 Hz even at the highest bias voltage setting.

fig:sipm_dark

3 Afterpulsing is another important aspect of SiPM performance. Afterpulsing
 4 increases noise and obstructs detection of late argon scintillation light. Results of
 5 the afterpulsing measurement performed on the SenSL C series, cooled down SiPM
 6 show very small afterpulsing fraction below 1% for most overvoltage values, as can
 7 be seen in Fig. ??.

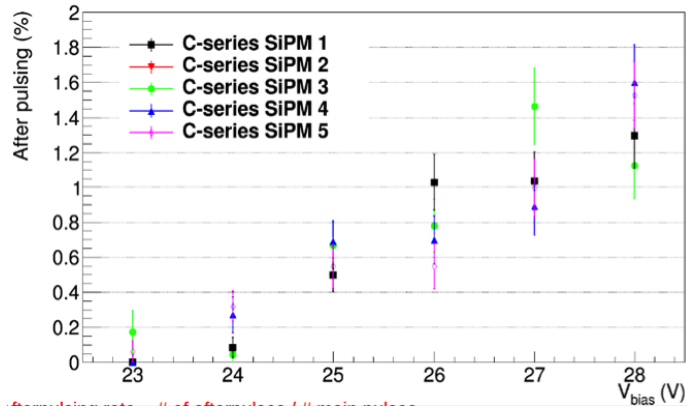


Figure 1.12: SenSL C series SiPM afterpulsing fraction for 5 different SiPMs, with system being completely cooled down.

fig:sipm_after

8 SenSL C series SiPMs were also tested for cross-talk. Cross-talk gives a measure

of the light hitting one pixel, also produces signal in adjacent pixels and effectively distorts the signal strength. Fig. ?? shows the test results. Cross-talk is a strong function of overvoltage which will be another criteria in choosing the operating over-voltage for the PD system.

Although, not presented here, SenSL B series SiPM MicroFB-600-35-SMT were also tested and satisfy our requirements, based on the tests conducted so far. However, we have not performed yet a full set of tests including mechanical integrity from thermal cycling and cross-checks.

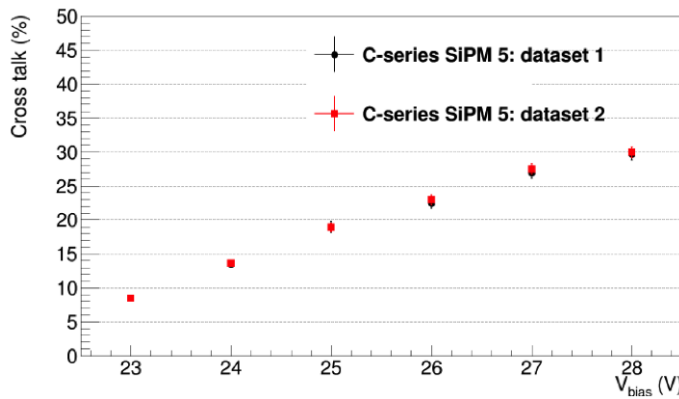


Figure 1.13: SenSL C series SiPM cross-talk measurement based on two separate runs in LN2. Cross-talk is a strong function of overvoltage and is very consistent between the runs.

fig:sipm_cross

In parallel with performance test, mechanical cryogenic tests were conducted where the number of cycles and time spent at LN2 temperature has been logged. This important test has started recently, but will involve testing a number of devices for extended period of time and examining mechanical status under the microscope along with performance tests.

Future steps involve increasing the testing sample of C series SiPMs and evaluating several alternatives to avoid the risk of sole source vendor.

1.5 Mechanical Support

Mechanically supporting the photon detector systems in the APA frames presented several challenges, including the need to support three different light collecting and wavelength shifting technologies in a package utilizing the same mounting features in

1 the APA frames, and the effects of varying thermal contraction of various materials
2 at 80 degrees Kelvin which complicated both light collector and SiPM mounting.

3 The baseline design for mounting the PDs into the APA frames calls for ten PD
4 modules, approximately 2.2m long, mounted roughly equally spaced along the full
5 length of the APA frame (Figure 1.14). The PD modules are read out using individual
6 twisted pair cable, one per SiPM. These cables (120 of them in the original baseline
7 design) are routed through the APA side tubes to a connector at the cold electronics
8 readout end of the APA. Initially it was decided that it would be too complicated
9 to design the APA frames to allow PD module installation following APA wire-
10 wrapping, so the PD modules were installed prior to this step in the installation
11 process. The Wavelength shifting elements in the light collectors of the PD modules
12 are sensitive to heat, humidity and most critically to exposure to ambient light,
13 which places significant requirements on the environment the APAs are assembled
14 and stored in this way, but initially it was decided this was the best option.

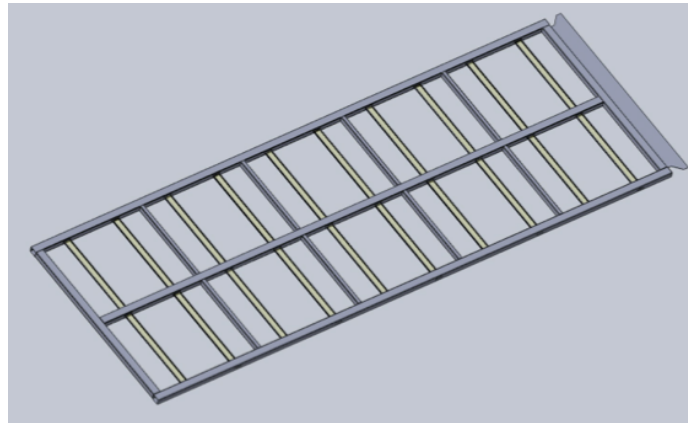


Figure 1.14: Full APA frame with ten photon detectors mounted inside the frame

fig:5.5-1

15 A universal PD frame assembly was devised to hold all three PD design variations
16 under consideration. Figure 1.15 shows an example of a short (400 mm long active
17 area) version of this frame manufactured for the 35t test, and Figure 1.16 shows
18 a mechanical assembly drawing of the frame system for one of the candidate light
19 collector choices. The frame consists of two plastic (acetal) end caps mounted to the
20 inside of the APA frame, joined by 10 mm diameter stainless steel tubes which run
21 the full width of the APA frame, providing intermediate support for the PD modules
22 as needed. The SiPM mount PCBs are incorporated into one of the end blocks,
23 along with the cable connections for the twisted pair cables. Due to the significant
24 variations in coefficient of thermal expansion between the stainless steel frame and

1 the plastic WLS elements, we expect a relative difference in thermal contraction of
2 1% at LAr temperatures. The far endblock assembly provides balancing forces to
3 the light collector elements as required to ensure these elements remain in straight
4 and in good contact with the SiPMs.

5 Testing of the PD mount scheme in many test setups (at IU, CSU and FNAL),
6 as well as experience APA assembly, have led to a re-evaluation of the PD mounting
7 scheme. The revised baseline has PD installation occurring following APA wire
8 wrapping, through slots left in the side of the APA frame (Figure 1.17). As shown
9 in the figure, the plan still calls for ten PDs per APA frame. Five of the PDs will
10 be installed through each side of the APA frame, and the cables for each of the
11 PDs will be routed to the cold electronics end of the APA inside the side tube the
12 PD was inserted through. Stainless steel c-channels mounted into the APA frames
13 prior to wire wrapping will guide and support the PDs during and after installation.
14 The PD will only be attached to the APA frame at one end, so the purely-plastic
15 PD module will be free to slide in the track to allow for the differential contraction
16 (Figure 1.18). Tests of 2.2m prototype assemblies of both fiber hybrid and the
17 LSU-proposed monolithic acrylic bar design in the CSU CDDF have demonstrated
18 significant promise. This installation scheme

19 Thermal contraction at cryogenic temperatures also complicates the mounting
20 of the SiPMs in the PD modules. The baseline sensL SiPMs are surface mount
21 components, with 4 0.5 X 0.5mm pads for making electrical contact. Reliability and
22 elevated dark count rate problems, as well as physical delamination of the SiPM front
23 face from the silicone substrate, were observed early in cryogenic testing of SiPMs,
24 and suspicion fell on the mechanical contact between the mounting PCB and the
25 SiPM itself.

26 Three different methods of making these electrical contacts: Soldering the SiPMs
27 directly to the PCBs (fig 5.5-6a), using commercial spring-loaded electrical contacts
28 or âAIJPogo pinsâI (Figure ??),

29 check ref

30 and soldering short wires to the SiPM pads and thence to the PCB (Figure ??).

31 check ref

32 Each of these methods provides assembly challenges, and cryogenic testing has
33 not suggested a clear choice so far. Testing and development are still underway to
34 resolve this issue.

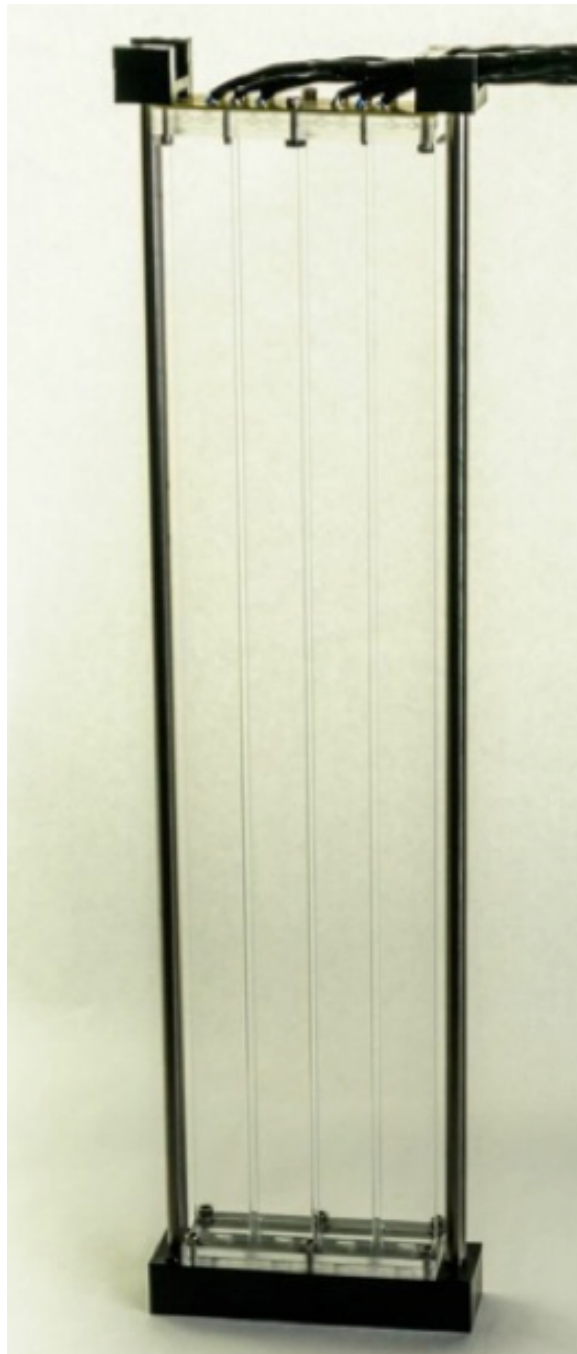


Figure 1.15: Photograph of 40 cm long bar-based prototype mounted in test frame

fig:5.5-2

Design for a Deep Underground Single-Phase LArTPC

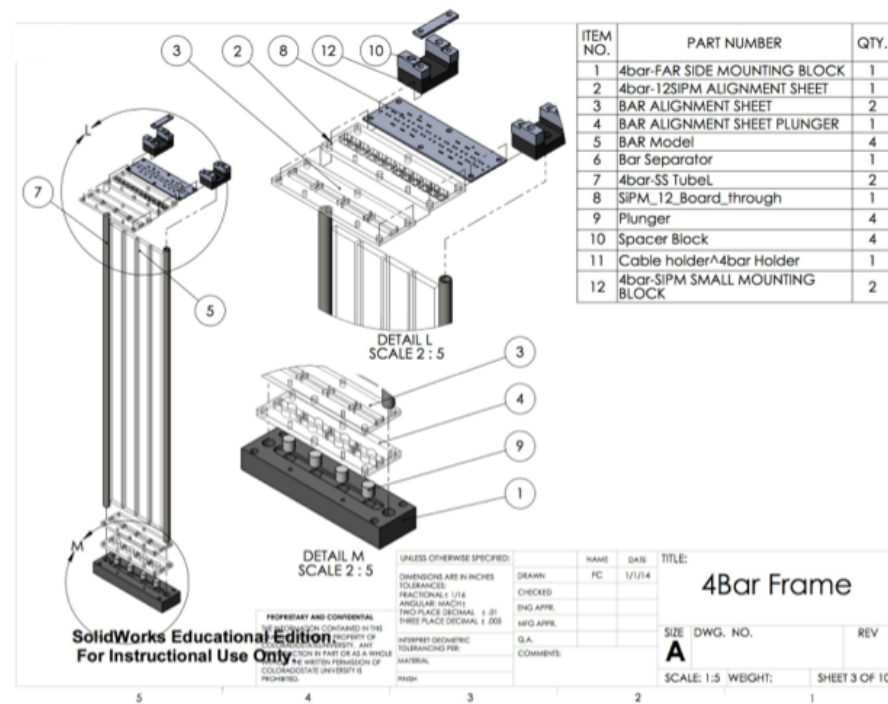


Figure 1.16: Mechanical assembly drawing of frame system

fig:5.5-3

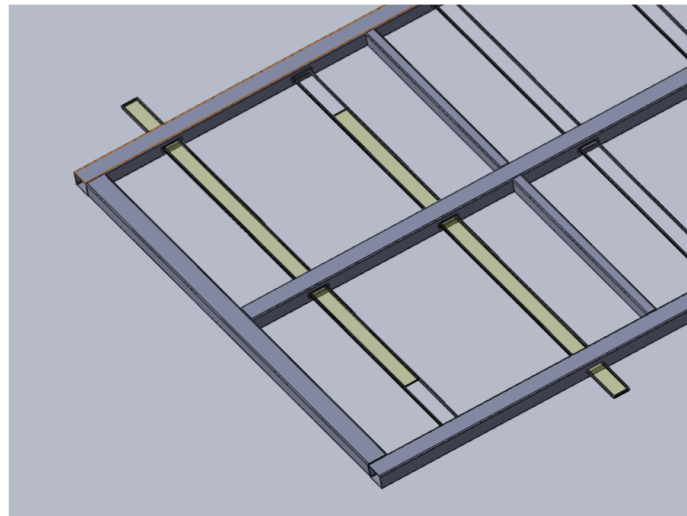


Figure 1.17: Blow up of APA fram showing PD insertion location

fig:5.5-4

Design for a Deep Underground Single-Phase LArTPC

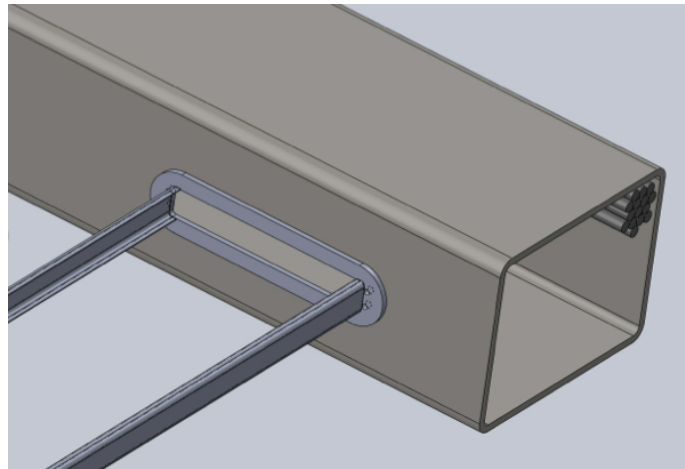


Figure 1.18: Slot and rail showing mounting location of photon detector

fig:5.5-5

1.6 Photon System Readout Electronics

sec_elec

1.6.1 Reference Design

Scintillation light from LAr comes from the two different excited states with lifetimes of about 6 ns and 1.6 μ s. Only a limited amount of light is collected by this system, so the electronics must be designed to collect the light from both excited states. A summary of the general requirements for the system, including requirements from a physics performance perspective, are given in Table 1.3.

Table 1.3: Physics requirements for the photon detector electronics

Performance Parameter	Target
Time Resolution	Better than 30 nS wrt event time zero ("t0")
Charge Resolution	0.25% photo-electron equivalent
Dynamic Range	$\sim \times 10$ better than detector (1000:1)
Linearity	Sufficient to resolve 1 photo-electron signals
Multi-Hit Capability	Sufficient to measure Triplet (late) Photons
Dead Time	Live up to 2 drift times either side of beam spill
Bias Control	0.1 V resolution up to 30 V per channel
Calibration	On-board Charge Injection
Timing	Events time-stamped using NO ν A Timing syst.

tab:fee_req

1 The plans for the electronics for the photon detection subsystem include a baseline
2 design with several options that remain R&D activities. There alternative implementations
3 of electronics are described in Section 1.6.2.

4 In the baseline plan, there are no front-end electronics in the cold volume. Instead,
5 the un-amplified signals from the SiPMs are transmitted to outside the cryostat on cables for processing and digitization, as shown in Figure 1.19. There are
6 advantages and disadvantages to this approach. The advantages are that the infrastructure required for inside the cryostat is reduced (power, data cables, precision
7 clocks, data protocols, etc.); reliability is improved (no single-point failures of multi-
8 channel devices inside the cryostat); serviceability and accessibility to the front-end
9 electronics are improved; and the need to develop cold electronics, possibly a custom
10 ASIC, is eliminated. The disadvantages are that the cable plant inside the detector is increased,
11 which can create mechanical challenges and installation difficulties; the flange board (warm/cold interface) is more complex; there are generally more
12 connectors in the system; and signal-to-noise considerations are more difficult. Generally,
13 the baseline design favors simplicity, reliability and reduced R&D time and costs, and also meets the performance requirements of the electronics.

18 No fig1 exists for: Block diagram of the photon detector signal processing system.

Figure 1.19: Block diagram of the photon detector signal processing system

fig:fig-e-1

19 In the 35-ton prototype, each SiPM signal was transmitted on an individual
20 shielded twisted-pair cable fitted with individual LEMO-style connectors. The bias
21 voltage was coupled onto the signal cable, using AC-coupling on the receiving end to
22 measure the SiPM signal. The use of high-quality cable with point-to-point connections
23 between an individual SiPM inside the cryostat and the front-end electronics
24 residing outside the cryostat, combined with good differential signal processing on the
25 receiving end, enabled the demonstration of the principle that single photo-electron
26 signals could be measured accurately without the need for cold electronics. In order
27 to address the problems with the cable plant as identified above, the following ideas
28 are being pursued:

- 29 • Ganging together of several SiPM outputs from a given PD detector into one
30 output cable. This increases the detector capacitance, affects the pulse shape,
31 and could spoil the timing resolution of the measurement. Also, the SiPMs
32 may have to be preselected, since there will be only one bias voltage for three
33 devices, and it may be important to match the over-voltage characteristics.

1 Studies are in progress to find a compromise between data precision and cabling
2 issues. One approach is to add a cold pre-amplifier if the ganging together of
3 several SiPMs result in performance that is too degraded to meet specifications.
4 The infrastructure requirements (cables, connectors, power, cold performance,
5 reliability, mechanical mounting, etc.) would have to be considered.

- 6 ● Use of multi-conductor, individually shielded pair cable. A candidate cable
7 containing four individually-shielded twisted pairs has been identified and tests
8 are in progress. The cable is in Teflon jacket, which should be acceptable for
9 use in LAr.
- 10 ● Use of mass-terminated connectors. Several candidate connectors for use with
11 the cable described above are being pursued.

12 The baseline plan assumes that three SiPM signals can be ganged together into
13 one readout channel. By using the multi-conductor cable with four twisted pairs,
14 this results in one cable per PD consisting of 12 SiPMs. The diameter of this cable
15 is xxx mm, which reduces the cable plant by $\sim x10$ compared to that used in the
16 35 ton detector. The cost of the connectors also decreases by $\sim x10$. Lastly, the
17 ease in making connections at the flange board will be improved by the use of a
18 mass-terminated connector.

19 In the baseline plan, the front-end electronics resides outside of the cryostat in
20 instrumentation racks. We have designed and built a custom module for receiving
21 SiPM signals, and performing signal processing in the front-end as preprocessing for
22 trigger and DAQ. The module is called the SiPM Signal Processor (SSP). An SSP
23 consists of 12 readout channels packaged in a self-contained 1U module. Each channel
24 contains a fully-differential voltage amplifier and a 14-bit, 150 MSPS analog-to-digital
25 converter (ADC) that digitizes the waveforms received from the SiPMs. The front-
26 end amplifier is configured as fully-differential with high common-mode rejection, and
27 receives the SiPM signals into a termination resistor that matches the characteristic
28 impedance of the signal cable. Currently there is no shaping of the signal, since
29 the SiPM response is slow enough relative to the speed of the digitization to obtain
30 several digitized samples of the leading edge of the pulse for the determination of
31 signal timing.

32 The digitized data is stored in pipelines in the SSP, for up to $\sim 13 \mu\text{s}$. The
33 processing is pipelined, and performed by a Xilinx Artix-7 Field-Programmable Gate
34 Array (FPGA). The FPGA implements an independent Data Processor (DP) for
35 each channel. The processing incorporates a leading edge discriminator for detecting
36 events and a constant fraction discriminator (CFD) for sub clock timing resolution.

- 1 Because the FPGA is programmable and accessible, it is possible to explore different
2 data processing algorithms and techniques, and even customize the readout for a
3 given type of event (supernova for example.) A picture of the module is shown in
4 Figure 1.20. A block diagram of the system is shown in Figure 1.21.

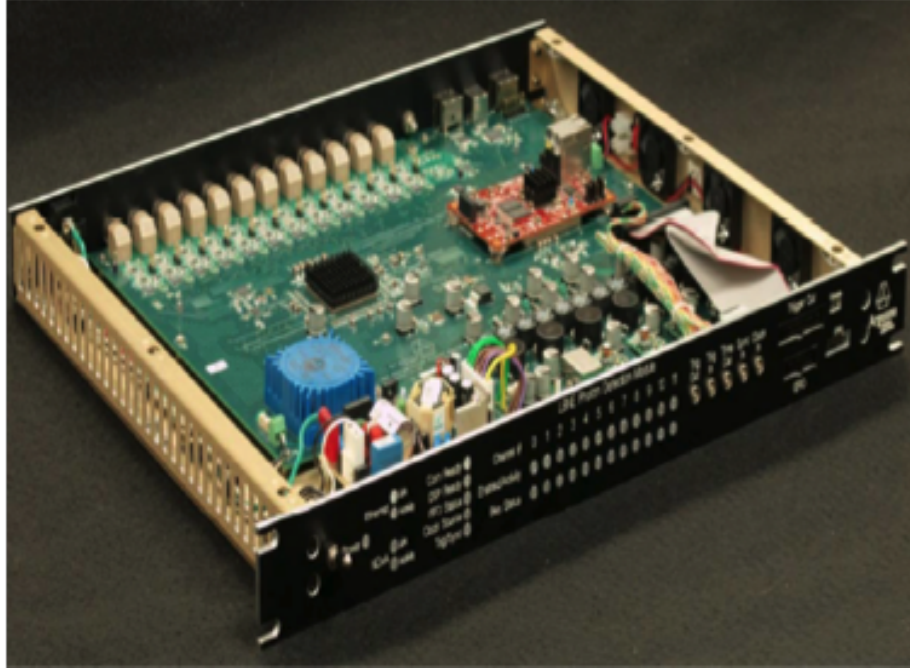


Figure 1.20: Picture of the SSP module

fig:fig-e-2

5 In the simplest mode of operation, the module can perform waveform capture,
6 using either an internal trigger or an external trigger. Up to 2046 waveform samples
7 may be read out for each event. When waveform readouts overlap the device can
8 be configured to offset, truncate or completely suppress the overlapping waveform.
9 Pile-up events can also be suppressed.

10 As an alternative to reading full waveforms, the DP can be configured to perform a
11 wide variety of data processing algorithms, including several techniques for measuring
12 amplitude, and also timing of the event with respect to a reference clock. All timing
13 and amplitude values are reported in a compact event record. Each data processing
14 channel stores up to 340 event records when not storing waveforms.

15 Generally, the SSP performs pipelined processing. The module has been designed
16 to support several different triggering schemes, including self-triggered, use of an
17 external trigger, or use an external gate to readout all events within a time-window.

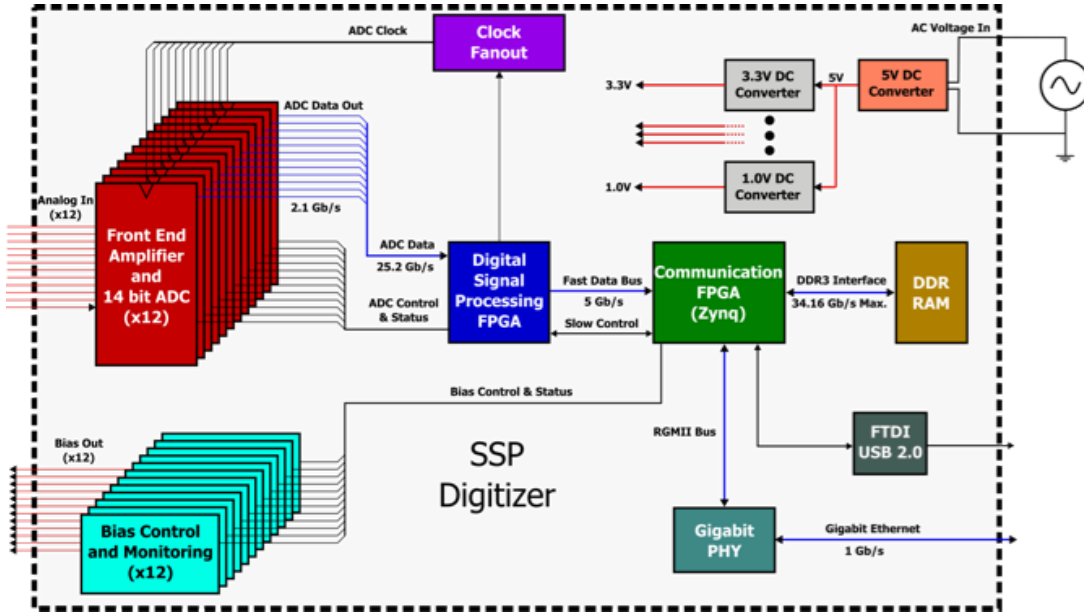


Figure 1.21: Block diagram the SSP module

fig:fig-e-3

1 In order for the events measured in the photon detector to be matched up with the
 2 corresponding events in the TPC, the front-end electronics attaches a timestamp
 3 to the data as it is acquired. The timestamp is unique, and has a correspondence
 4 with the timestamps in the TPC electronics processing. The timestamp in the SSP
 5 is applied to the event data as it is digitized, and becomes part of the data as the
 6 processing proceeds. In the case where zero-suppression and data sparsification are
 7 used, the timestamp on accepted data remains intact. To achieve this, the TPC
 8 and PD electronics must be synchronized, including timestamp counter resets, and
 9 a known and stable calibration between the corresponding timing resolution of the
 10 ADC conversion in the two systems. The electronics has been designed to support
 11 a full interface to the NO ν A timing system, which is the baseline timing system for
 12 the experimental prototypes.

13 A Xilinx Zynq FPGA, onboard the MicroZed system-on-module, handles the slow
 14 control and event data transfer. The SSP has two parallel communication interfaces;
 15 USB 2.0 and 10/100/1000 Ethernet. The 1 Gb/s Ethernet supports full TCP/IP
 16 protocol. The module includes a separate 12-bit high-voltage DAC for each channel
 17 to provide up to 30 V of bias to each SiPM. The module also feature charge injection
 18 for performing diagnostics and linearity monitoring, and also voltage monitoring.

19 In tests to date, the SSP is capable of measuring single photo-electron signals

1 coming from the SiPMs over a cable length of 30 meters when the SiPMs are operated
2 at LAr temperatures. The timing resolution of the signals has been measured to be
3 better than 3 ns. The full-differential signal processing in the front-end circuitry is
4 important in achieving this result.

5 The SSP is self-contained in that it receives 60 Hz, 120V power, and has internal
6 linear and DC/DC power supplies for generating the DC voltages needed for the
7 instrumentation, as well as the bias voltage for the SiPMs. The SSP is packaged in
8 a 1U, rack-mountable package. For the 35-ton prototype, the racks are located near
9 the ports on the top of the cryostat.

10 **1.6.2 Alternatives**

sec_alt
11 In the baseline design of the PD electronics, the approach was taken to have no
12 electronics inside of the cold volume. This results in a large number of cables and
13 connectors. Other experiments using liquid argon have successfully implemented
14 cold TPC electronics, thereby significantly reducing the cable plant that must come
15 through the cryostat.

16 This approach has challenges in power distribution, heat dissipation, and the
17 performance of front-end electronics in LAr. To address serviceability, the cold elec-
18 tronics might be realized in a modular way and situated just below the flange in
19 the cryostat so that it can be accessed in the event that repair is needed. To this
20 end the zero-suppression will be important to avoid high data rates depending on
21 the number of readout channels needed. A way to realize the cold zero-suppression
22 would be to implement a cold FPGA (or an ASIC, yet to be developed). So far the
23 cold FPGAs have had mixed results in tests.

24 An alternative approach would be to perform an “analog zero suppression” with a
25 constant-fraction discriminator and then gate the signal and digitize warm, in which
26 case the complication with encoding the particular channel has to be addressed.
27 The significant challenges in this technique include power dissipation, the increased
28 possibility of contamination of the LAr, and extended infrastructure requirements
29 that must reside in the cold volume. The virtue is that this can significantly reduce
30 the number of signal penetrations into the cold volume.

31 The electronics for the photon detector of LBNE uses fast (direct) digitization of
32 the SiPM pulses. Another option for the front-end electronics is to use pulse shaping.
33 Instead of digitizing the full bandwidth of the SiPM signal, the pulse is shaped using
34 analog filtering techniques, generally producing a pulse with a prescribed shape with
35 a peak that is proportional to the total amount of charge. By measuring the peak,
36 both amplitude and pulse timing can be obtained. Since the pulse response follows

1 a known transfer function, the pulse peak can be obtained using slower synchronous
2 sampling, or using asynchronous sampling through the use of peak detection and
3 constant fraction discrimination.

4 In either case, the data can be processed by an FPGA using algorithms optimized
5 for the application. In particular, assuming that a sufficient number of samples are
6 obtained of the shaped pulse, a chi-square comparison of the shape to the ideal
7 pulse can be used to determine pulse corruption, or event identification. As with
8 direct digitization, the digitization clock and timestamp can be synchronized using
9 an external clock source. The data can be read out in a similar manner, using USB
10 2.0 or 10/100/1000 Ethernet. The virtue of this approach is that a slower ADC can
11 be used, reducing power consumption, and also reducing data load and the speed
12 of readout links. The technique does trade bandwidth for shaping, making timing
13 and pile-up issues more important. This can result in the interpretation of the pulse
14 shape becoming more complex than direct digitization. Generally, the pulse shaping
15 circuitry is also less expensive than the direct digitization technique, assuming similar
16 performance requirements.

17 Another option for the photon system readout would include the use of an Application
18 Specific Integrated circuit (ASIC) as a way to reduce cost. The large channel
19 count in a real detector system is such that the production cost of the system could
20 be greatly reduced. Often, the cost of development of an ASIC from scratch is
21 quite high, of order \sim 400K, and can take \sim 1 to 2 years for development, so cost
22 and schedule must be weighed carefully. However, other benefits from the ASIC
23 approach include reduced space requirements for circuitry on the front-end, lower
24 power dissipation, and specialized functionality in the front-end chip.

25 There exist several ASICs that have been designed over the last few years especially
26 for SiPM readout. One could potentially explore the functionality and performance
27 of these designs, and evaluate their suitability for LBNE. This option might
28 be used either for warm or cold electronics. Direct digitization has the virtue of being
29 straight-forward from a circuit design perspective. By taking advantage of modern
30 high-bandwidth OP amps, high-speed, high-rate ADCs, and powerful FPGAs with
31 high-speed serial links, it is possible to obtain 14-bit dynamic range digitization with
32 \sim 1 ns timing resolution. By reading all of the samples into an FPGA having a deep
33 buffer, digital signal processing techniques can be employed using the programmable
34 logic, offering powerful analysis algorithms that can be developed in time. The technique
35 generally has higher power consumption and tends to be more expensive than
36 simpler instrumentation techniques.

1.7 Photon Detector Calibration

1 sec_pd_calib
2 The photon detector calibration is a part of a larger calibration plan that covers all
3 aspects of an LAr detector calibration, and includes methods to convert collected
4 charge to initial particle's energy, as well as calibration techniques to convert col-
5 lected scintillation light into estimate of particle's interaction time, energy, and a
6 track/vertex location for each event.

7 As already described, the baseline for the scintillation photon detectors assumes
8 employment of acrylic light collection paddles to reduce the required costly photo-
9 cathode area. Several photon detector designs are presently being developed and are
10 being tested in small dewars. Since each of these new elements has not yet been
11 tested in a large-scale TPC, the 35-ton LArTPC prototype is being constructed to
12 provide essential design validation.

13 The current FD designs are anticipated to have sufficient sensitivity to provide
14 event timing information for atmospheric neutrino and proton decay channels. How-
15 ever, it will not provide high efficiency down to the 5-MeV neutrino energy level
16 desired by the supernova program. This would have the impact that the event re-
17 construction energy resolution would be 20% rather than 5% achievable with the
18 event time determination from a photon detector able to operate efficiently at a suf-
19 ficiently low energy threshold. The improvement in physics will be studied in the
20 near future but a substantial effort in development of improved detection techniques
21 is desired.

22 In the absence of precise physics requirements for the photon detector system
23 and in order to support R&D activities on the photon detector development it was
24 decided that the photon detector should provide a time stamp to determine the time
25 of occurrence of an event (so called "time zero") with an accuracy much better than
26 1 s

27 fix

28 .

29 Items relevant to the photon detector calibration are the fast and slow components
30 of the light, photon propagation including scattering and reflections, impact of N₂,
31 E-field strength, as well as the energy range of interest. A calibration system that
32 addresses the issues listed above has to be both comprehensive and cost-effective,
33 and has to be tied to the overall calibration system that includes both charge and
34 scintillation light calibration techniques. Such a system will be designed in the future.

35 To support the PD R&D phase we designed a light-flasher based calibration
36 system that will serve to monitor the relative performance and time resolution of the
37 system. In particular, for anticipated 35-ton performance tests we need to evaluate

1 relative efficiencies of multiple light collection techniques in order to be able to down-
2 select an optimal light readout technology. The system that meets these requirements
3 will consist of a set of LEDs as light sources or a laser with a VUV wave-length,
4 coupled to quartz fibers, thus transmitting light from outside the detector volume
5 to desired locations at the CPA within a TPC. Therefore we will equip the 35-ton
6 detector with LEDs located and fired externally, with fibers running into the cryostat,
7 to diffusers that will emit light from the CPA to the APA.

8 For the 35-ton cryostat at the surface at Fermilab it will be complementary
9 to cosmic ray muon tracks as means of calibration. In terms of light sources the
10 measurements should be performed with an UV (245-375nm) light source. The UV
11 light mimics physics starting from the wavelength shifter conversion, light guide
12 propagation, photo-sensor detection and FEE readout. The external light-flasher
13 calibration system is designed under following assumptions:

- 14 • simple to implement (no active components within PD/APA, such as LEDs or
15 fibers mounted within APA).
- 16 • less-intrusive (less material within detector in terms of fibers, then equipping
17 each PD frame with individual fiber).?
- 18 • provide a benchmark light-based reconstruction with the use of localized light
19 sources distributed throughout the detector volume.
- 20 • has a potential to be adapted for deployment in a large Far Detector in the
21 future

22 We describe the system in Figure 1.22.  The system consists of a 1U rack
23 mount Photon Detector Calibration Module (PDCM) sitting outside the liquid argon
24 cryostat. The module generates light pulses that propagate through a quartz fiber-
25 optic cable to diffusers at cathode-plane (CPA) to distribute the light uniformly
26 across the photon detectors mounted within anode plane (APA). There are 5 diffusers
27 on the CPA plane: one in the center and four diffusers close to the CPA corners, as
28 shown in Figure 1.23. 

29 The PDCM module layout is shown in Figure 1.24. The ANL photon calibration
30 module is based on a re-purposed SSP unit. An SSP board will be repackaged into a
31 deeper rack mount chassis that will accommodate a new internal LED Pulser Module
32 (LPM) and an additional bulk power supply. The LPM utilizes five digital outputs
33 to control the LPM pulse and its duration (arrows in black). These LVDS outputs
34 are derived from the charge injection control logic within the SSP's FPGA. The
35 even channel SiPM bias DACs are repurposed to control the LPM pulse amplitude

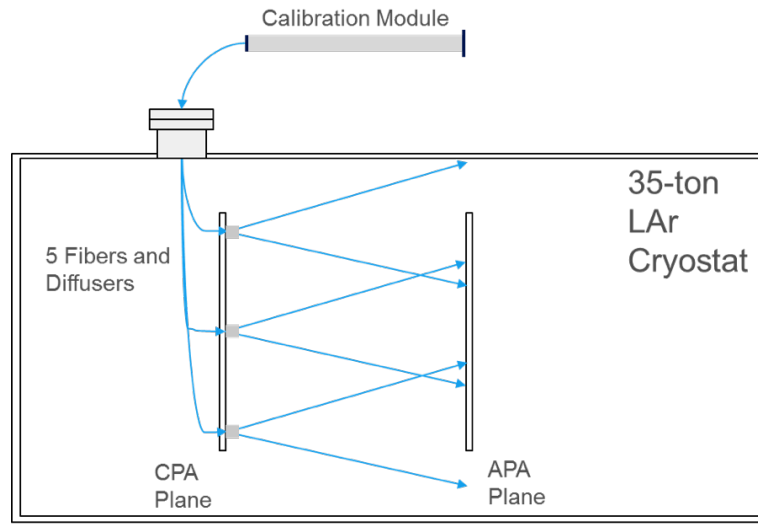


Figure 1.22: Concept of the UV-light calibration system for the photon detector in liquid argon

fig:fig-c-1

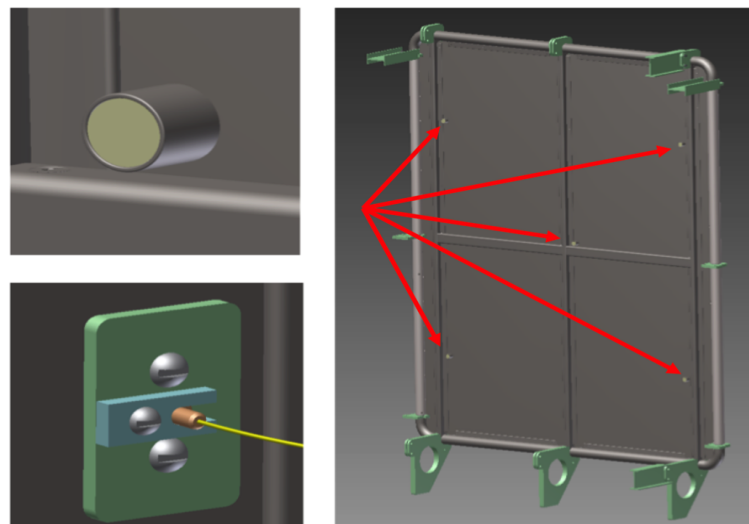


Figure 1.23: The diffuse light is emitted from diffusers (top left figure) mounted at five CPA locations, indicated by arrows (right figure). The UV light from the PDCM to diffusers is transported through quartz fiber (lower left figure).

fig:fig-c-2

1 (arrows in red). The adjacent odd channels are used to readout a photodiode which
 2 is used for pulse-by-pulse monitoring of the LED light output. The output of the
 3 monitoring diode is used to normalize the response of the SiPMs in the detector to
 4 the calibration pulse

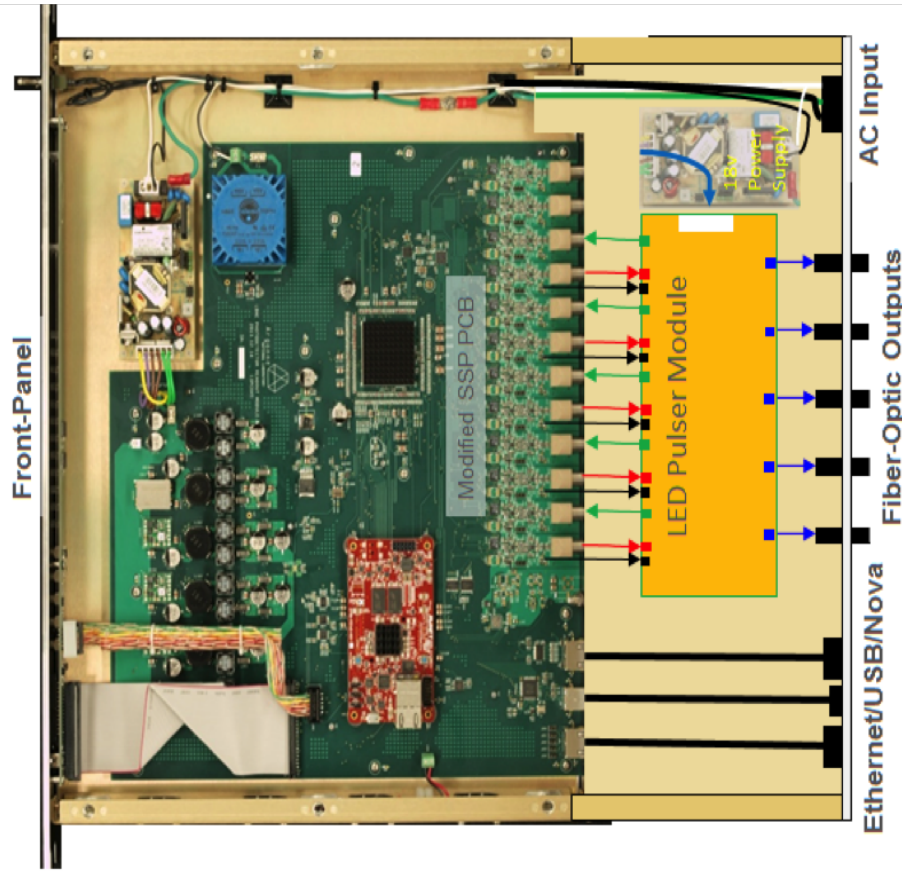


Figure 1.24: Photon detector calibration module (PDCM) layout

fig:fig-c-3

5 For the 280 nm light we have performed a simulation of the designed diffuse
 6 light calibration system using TracePro, a generalized 3-D light ray-tracing program
 7 with the ability to include bulk optical properties such as absorption, fluorescence,
 8 birefringence in addition to surface properties such as scattering and reflection. Figure
 9 ^{Tip Fig-c-4} 1.25 shows simulated light distributions of at the 35-ton APA for the cases of
 10 the VUV light emitted by either the central diffuser only (left figure), or by outer
 11 four diffusers simultaneously (right figure). A full Geant4 based simulation of the
 12 detector will be used in the future. Using the preliminary data with the 35-ton style

1 light guides (indicating 0.5% efficiency for number of photo-electrons per incident
 2 128 nm LAr scintillation photon 50 cm from the light guide), we estimate for 280
 3 nm light to observe 15 photo-electrons per single SiPM channel when the light is
 4 emitted from the single central diffuser in 13 ns long pulses. Similarly, we expect
 5 about 100 photo-electrons observed by a single SiPM channel when 280 nm light is
 6 emitted in 100 ns long pulses from the four outer diffusers at once.

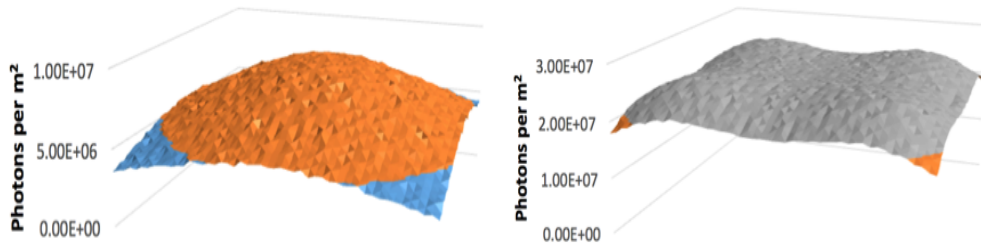


Figure 1.25: Simulated light distributions of the 35-ton APA for the cases of the VUV light emitted by either the central diffuser only (left), or by outer four diffusers simultaneously

fig:fig-c-4

7 In the LBNE prototypes (i.e. in 35-ton) and in Future Far Detector it will be im-
 8 portant to check if photon-detector components are functioning properly at various
 9 stages of the detector operation. Periodic light source deployments will monitor the
 10 systems stability as a function of time. A change in relative difference of UV light
 11 responses will indicate towards potential wave-length shifter instability, changes in
 12 SiPM gain and collection efficiencies. Much of the same monitoring is expected to be
 13 doable with cosmic rays in the 35-ton (at surface), with periodic LED/laser calibra-
 14 tion runs complemented with cosmic-ray data tracked with an external hodoscope.
 15 With the 35-ton detector one could use a well-defined muon trajectory defined by the
 16 hodoscope geometry and monitor the number of PEs per MeV of deposited charge.
 17 The number of PEs per PD channel from the well-defined muon track could be used
 18 as a calibration constant. However, for the deep underground LBNE the cosmic ray
 19 flux may inadequate for timely monitoring of the photon detectors. With the 35-ton
 20 detector we have planned two sets of calibration runs:

- 21 1. Calibration runs with four outer diffusers run simultaneously, in order to
 22 -measure response of PD channels in multi-PE range and get integrated number
 23 of event samples for each channel (for maximum light output)
 24 -test of the dynamic range from 1PE to maximum number of PEs.
 25 -repeat runs periodically to trace any changes in channel response.

- 1 2. Runs with central diffuser only, in order to
- 2 -perform initial calibration runs that will reveal malfunctioning channels, if
- 3 any.
- 4 -timing measurements with the 10-50 ns pulses, verify time resolution of the
- 5 PD system.

6 The controlled source of light described here will be used to perform a relative
7 ?t0? calibration, where the ?t0? could be absolutely calibrated with the use of the
8 cosmic ray triggers available with 35-ton detector. Effects that contribute to a finite
9 time resolution and relative time offset of PD channels include scintillation time
10 constants, photon conversion with wave-length shifter, photon propagation through
11 PD paddle, SiPM jitter, and FEE resolution. Most these effects are constant and
12 can be individually measured on the bench, so the LED flasher system will monitor
13 overall stability of the photon detector. To go beyond the current R&D phase one
14 needs detailed MC simulations of light production, propagation, and detection to
15 perform comparisons of reconstruction performance against prototype data in terms
16 of calorimetric energy and position reconstructions for measured event tracks. Future
17 light collection systems will aim to maximize the active area of the light guide bars, to
18 achieve a high photon detection efficiency with an optimized timing and granularity
19 required for improved position resolution. As in the case with the TPC charge
20 calibration we will need to evaluate what may be achieved with expected cosmic ray
21 muons and Michels, π^0 , and natural radioactivity events (such as ^{39}Ar with end-point
22 energy of about 500 keV).

23 1.8 Installation

24 Installation of the photon detectors is one of the most significant factors driving the
25 mechanical design. As discussed above, our initial thought was to install the PDs
26 and run the SiPM twisted pair cable down the frame side tube prior to wire-wrapping
27 the APA. Following our experience with the environmental controls (primarily UV
28 filtered light) required by the PDs, as well as the difficulties in dealing with the
29 PD readout cable ends during wire-wrapping, it was decided to change the baseline
30 to include inserting the PDs following wire wrapping. In addition to relaxing the
31 physical constraints on the wire wrapping, this also relaxes a schedule connection
32 between the APA and PD fabrication. It is not necessary to install the PDs into the
33 APA frames until shortly prior to installation of the APAs into the cryostat.

34 As noted above, and shown in Figure 1.17, a total of 10 PDs are installed into
35 each APA frame, with 5 coming in from each side. The installation will occur with

1 the fully-assembled APA frame lying flat on an insertion station table. Prior to
 2 installation, the PD cable bundle will be inserted into the APA side tubes. The
 3 cable bundle will be pre-assembled prior to installation such that the end of each
 4 cable will terminate at the correct slot for the PD to be connected. Our baseline
 5 cable design has also been modified to a single cable with 4 individual twisted pairs
 6 in a single jacket, so each APA side tube will only require 15 cables (3 per PD, 30
 7 per APA). These cables extend approximately 30cm past the end of the APA tubes
 8 at the cold electronics end of the APA, and following installation of the APA into
 9 the cryostat are connected to long-haul cables for the run to the readout electronics
 10 (see Figure ??) fig:5.8-1

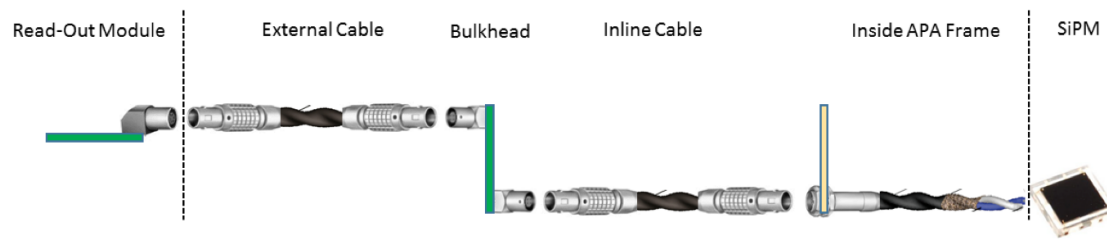


Figure 1.26: Cable assembly for each photon detector readout channel.

fig:fig:5.8-1

11 Following this step, 5 PDs will be inserted into the APA through one side frame,
 12 with connections being made between the twisted pair cables and the SiPM PCB
 13 just as the readout end of the detector enters the tube (See Figure ??). The PD
 14 is then inserted the last 10cm fig:5.8-2 into the frame, and affixed to the inner surface of
 15 the APA tube (See Figure ??). The process is then completed for the 5 PDs to be
 16 inserted from the opposite side.

17 Following insertion of the PDs, the environmental controls required for the PD
 18 WLS materials (UV filtering, temperature and humidity control) will need to be
 19 observed for the entire APA.

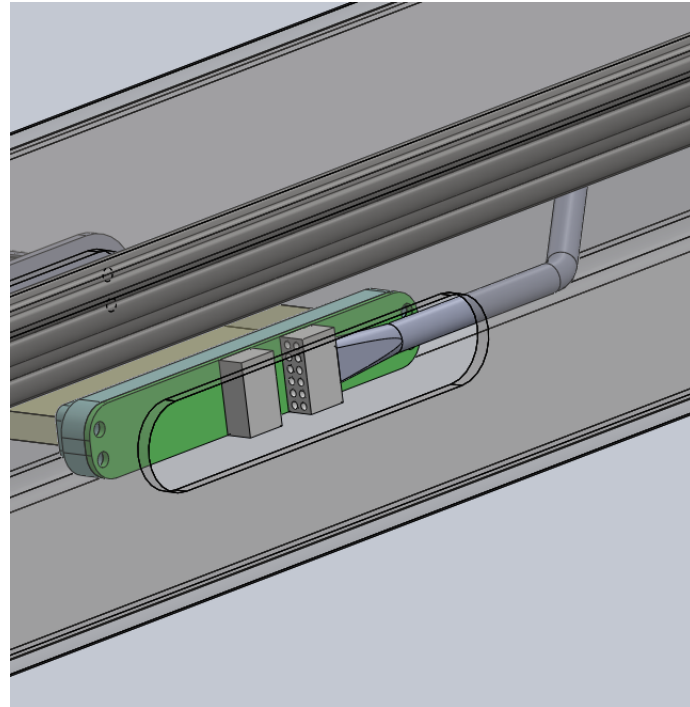


Figure 1.27: Connection between the PD twisted pair cable and SiPM mounting board.

fig:fig:5.8-2

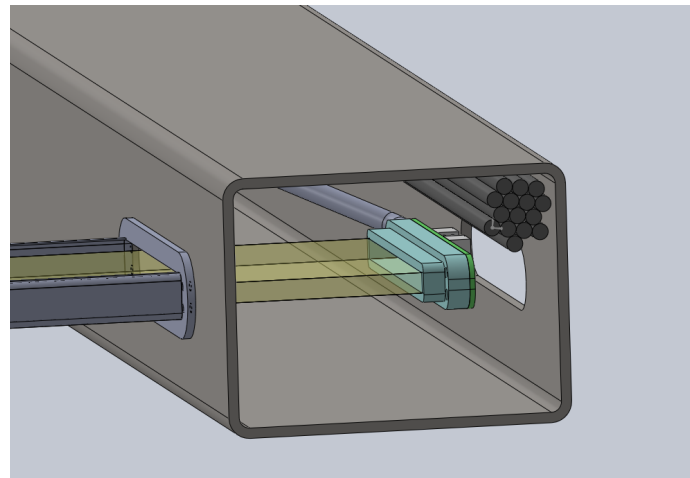


Figure 1.28: Insertion of one PD paddle

fig:fig:5.8-3